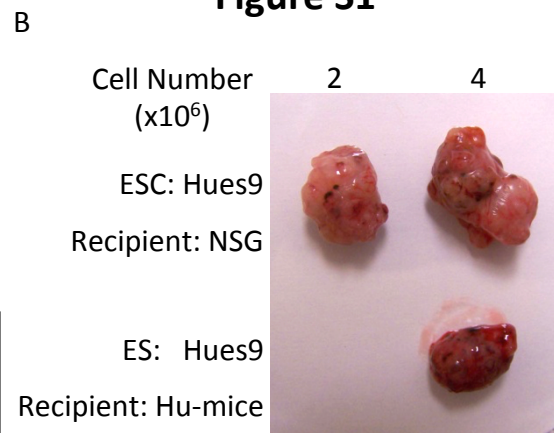
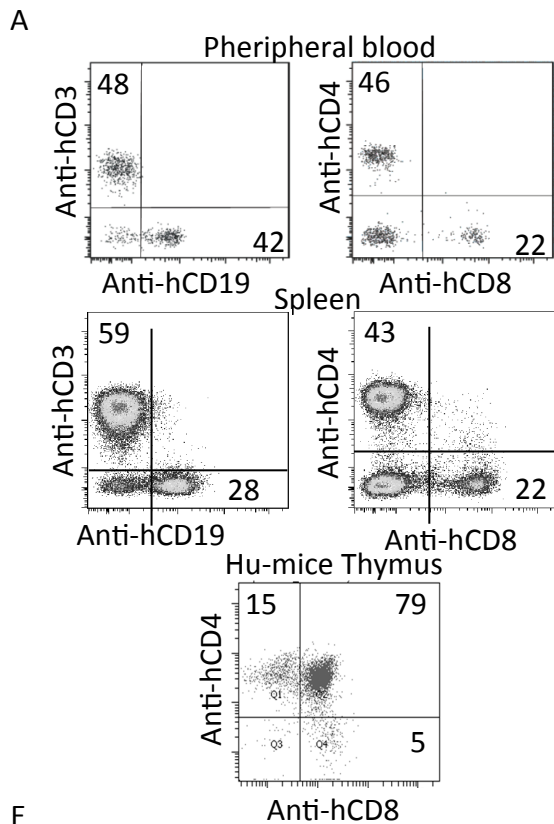


**Figure S1**



**C**

Surviving rate of grafts and T cell infiltration in SCID and HuSCID mice by Hues (p33-p38)

Recipient (Cell number)	Cell lines (Passage#)	Visible teratoma	CD3 infiltration
NSG (2X10 <sup>6</sup> )	Hues9	6/6	0/6
NSG (4X10 <sup>6</sup> )	Hues3	6/6	0/3
NSG (4X10 <sup>6</sup> )	Hues8	6/6	0/6
Hu-mice (2X10 <sup>6</sup> )	Hues9	1/6	1/1
Hu-mice (4X10 <sup>6</sup> )	Hues9	4/8	4/4
Hu-mice (4X10 <sup>6</sup> )	Hues3	6/6	6/6
Hu-mice (4X10 <sup>6</sup> )	Hues8(p33)	4/4	4/4
Hu-mice (4X10 <sup>6</sup> )	Hues8(p38)	4/4	4/4

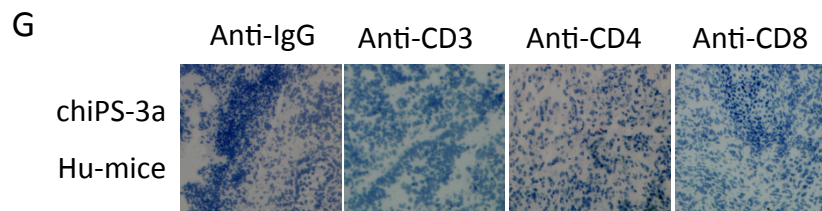
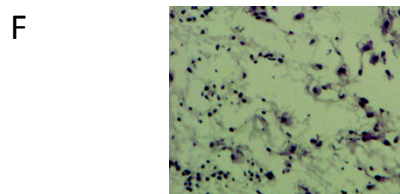
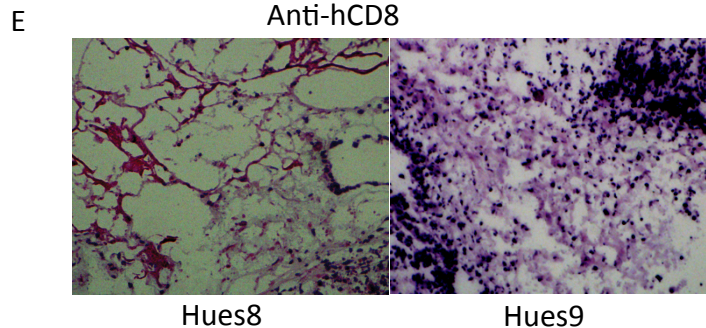
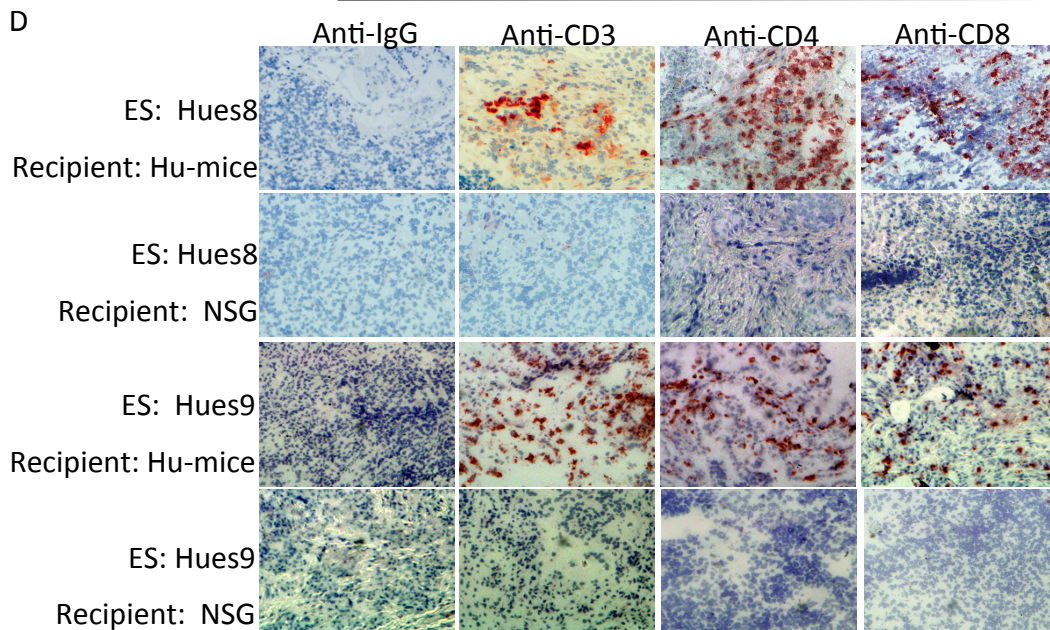


**Figure S1.** Establishment of functional Humanized mice (Hu-mice) reconstituted with human immune system to study immunogenicity of cells derived from human PSCs. (A) Hu-mice, reconstituted by transplanting human fetal thymus, fetal liver and CD34<sup>+</sup> cells into NSG mice, can efficiently develop human immune system including CD4<sup>+</sup> and CD8<sup>+</sup> T cells as well as CD19<sup>+</sup> B cells. Peripheral blood, spleen and transplanted thymus of Hu-mice were analyzed by flow cytometry for the presence of T and B cells. (B) hESCs can efficiently form teratomas in NSG mice but not in Hu-mice reconstituted with allogenic human immune system. (C) The summary of the efficiency of teratoma formation and T cell infiltration into the teratomas formed by allogenic hESC lines in Hu-mice. For each teratoma assay in Hu-mice, each hESC line was transplanted subcutaneously into the Hu-mice generated from one donor. (D) Extensive infiltration of T cells into the teratomas formed by Hues8 and Hues9 in the same cohorts of Hu-mice. Representative images are shown. (E) Extensive necrosis is evident in the teratomas formed by hESCs in Hu-mice. (F) Local necrosis was found in hiPSC-derived teratomas formed in Hu-mice with autologous human immune system. (G) Serial sections of one teratoma formed by chiPS-3a hiPSCs in Hu-mice with autologous immune system failed to identify any T cell infiltration. Related to Figure 1.

**Figure S2**

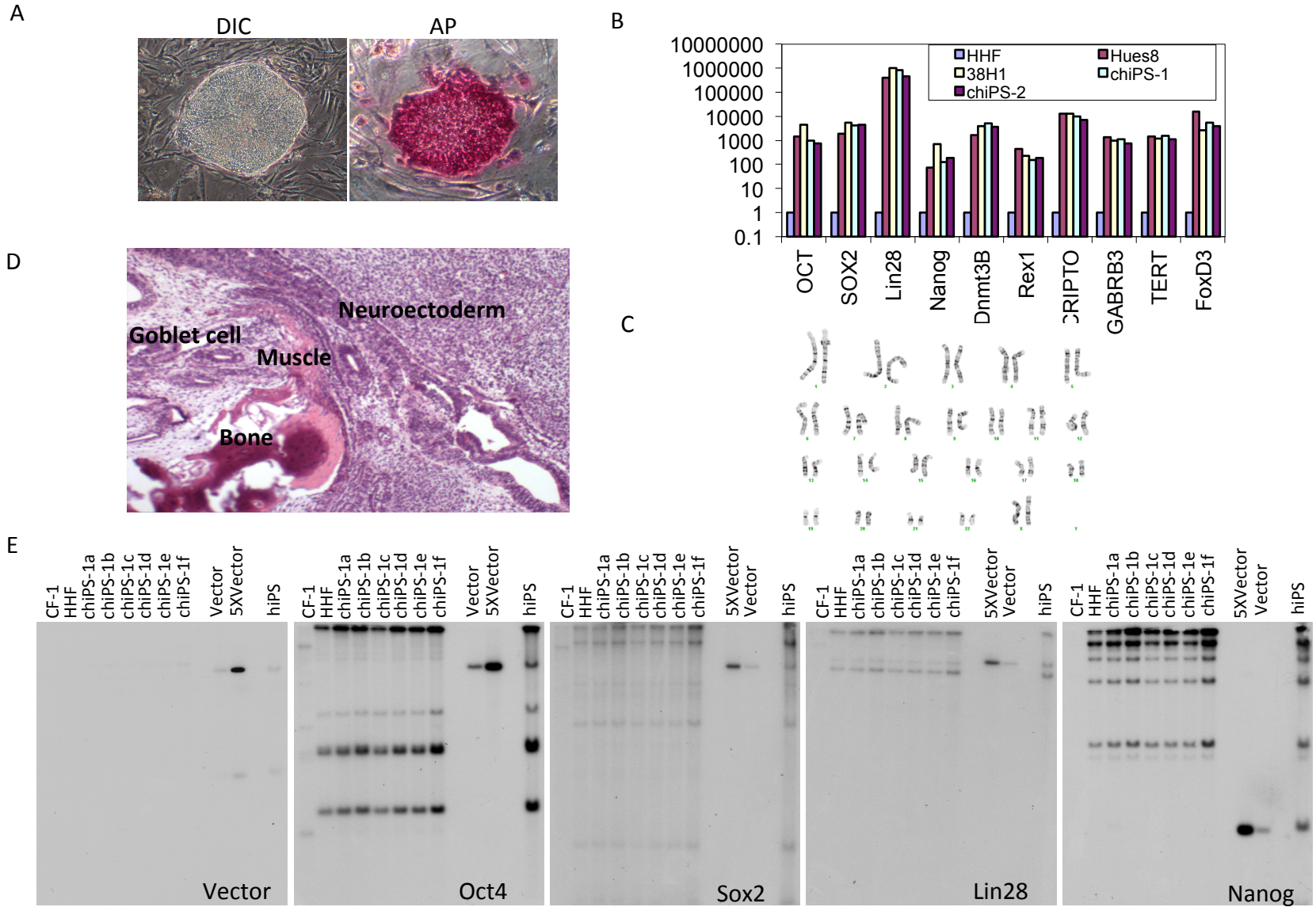


**Figure S2.** Generation of integration-free human iPSCs. (A) The hiPSCs (chiPS-1a) are alkaline phosphatase positive. (B) The hiPSCs (chiPS-1a and chiPS-2a) express pluripotency markers to the similar levels as hESCs. (C) The hiPSCs (chiPS-1a) have normal karyotype. (D) The hiPSCs (chiPS-1a) can form well-differentiated teratoma in NSG mice. (E) Southern blotting analysis indicates no random integration of the episomal vectors in some independent hiPSC clones (chiPS-1a, b, c, d, e and f). Genomic DNA derived from hiPSCs was digested with BamHI and hybridized to various probes that cover the entire episomal vector. Related to Figure 2.



**Figure S3**

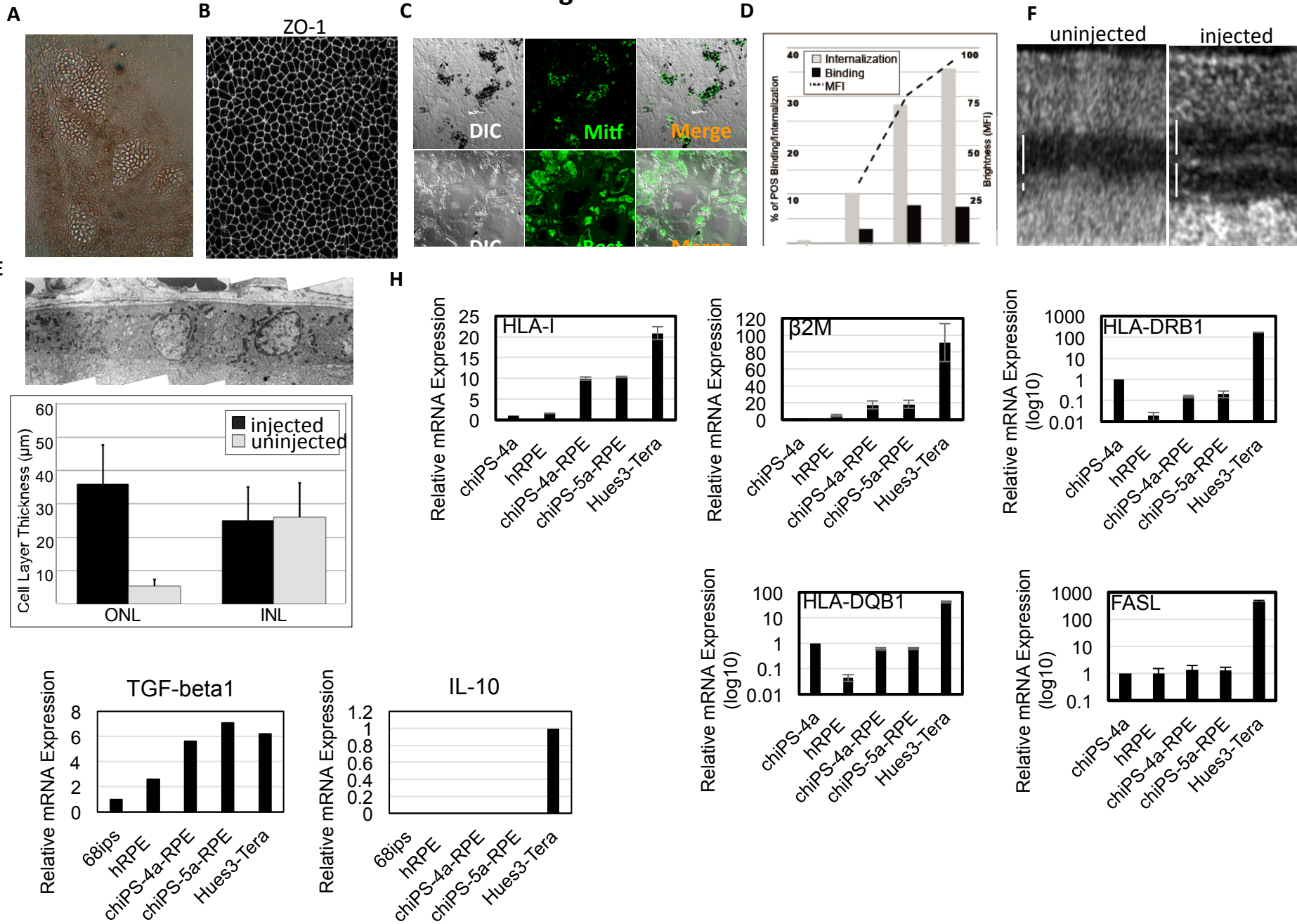




**Figure S3.** Characterization of hiPSC-derived RPEs. (A) hiPSC-RPE are pigmented in culture and form “domes.” The domes demonstrate the RPE cells are tightly coupled and are pumping water and ions in a vectorial fashion. (B) hiPSC-derived RPEs have the right morphology as revealed by ZO-1. (C) hiPSC-derived RPEs are positive for Mitf and Best (Bestrophin). (D) Based on flow-cytometry analyses, cultured hiPSC-RPE exposed to FITC labeled porcine POS over several hours bind the POS (black bars), and internalize the outer segments (gray bars). MFI values in this assay (dashed line) represent the number of POS internalized. (E) Pigmented hiPSC-RPE were injected into the subretinal space of albino RCS rats. Four weeks after implantation, the eyes were enucleated and processed for electron microscopy. At regions adjacent to the injection site, the hiPSC-RPEs formed a monolayer and are polarized (long apical processes and basal infoldings can be observed). (F) In vivo optical coherence tomography imaging reveals the architecture of the RCS retina. In one uninjected eye of an 8 week old RCS rat the outer nuclear layer (ONL) that contains photoreceptors is basically absent. In the contralateral eye of the animal in which hiPSC-RPE were injected, the ONL can be detected. (G) Quantification was performed in three animals and demonstrated robust rescue of the ONL (6.75 fold increase;  $p=0.02$ ) while the thickness of the inner nuclear layer is not affected ( $p=0.50$ ). (H) The expression of HLA-I,  $\beta$ 2M, HLA-DRB1, HLA-DQB1, and FASL in hiPSC, human primary RPE, hiPSC-derived RPE and teratoma, was detected by qPCR. (I) The expression of TGF- $\beta$ 1 and IL-10 in human primary RPEs and hiPSC-derived RPEs. Related to Figure 3.

Figure S4

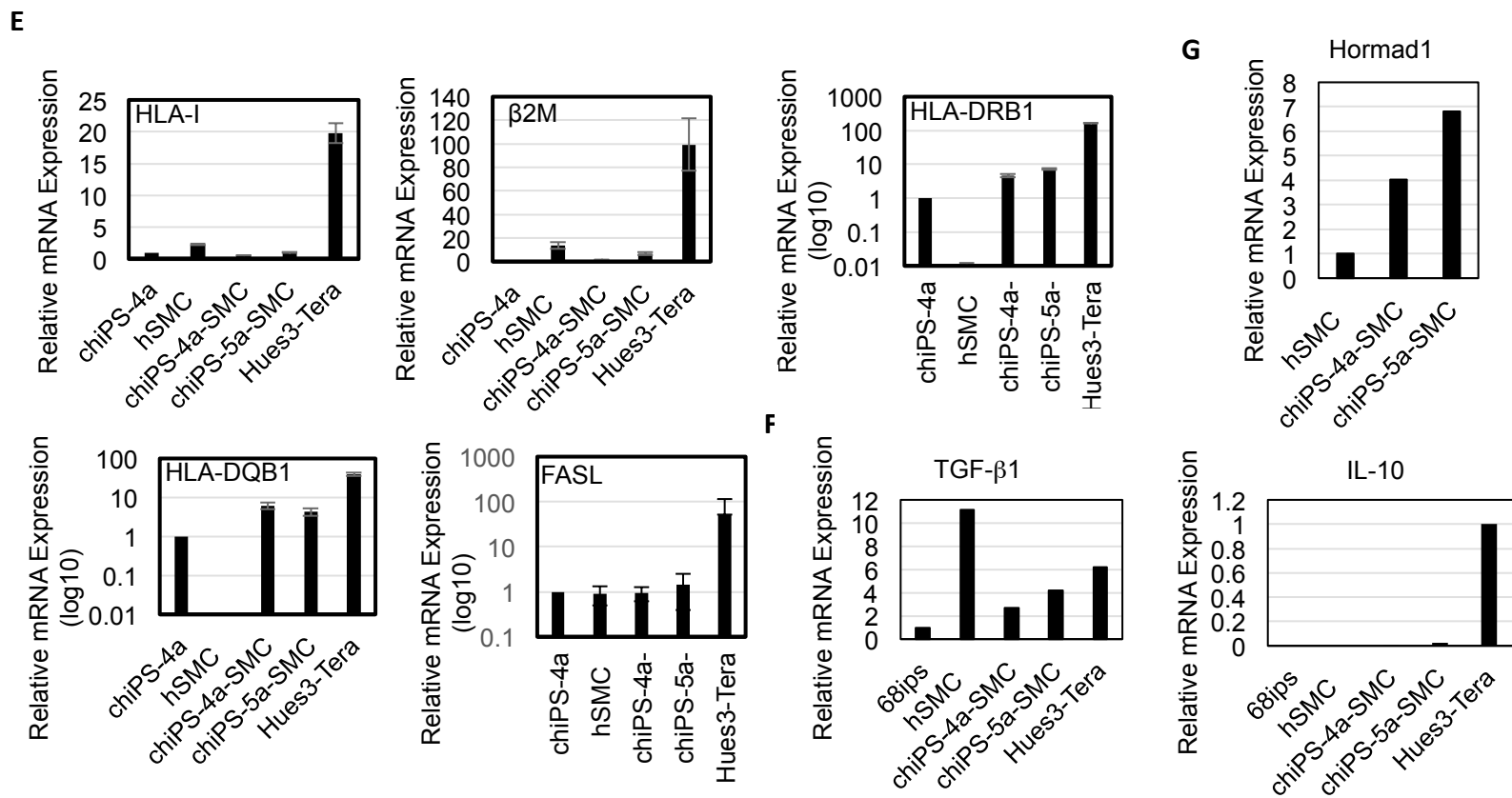
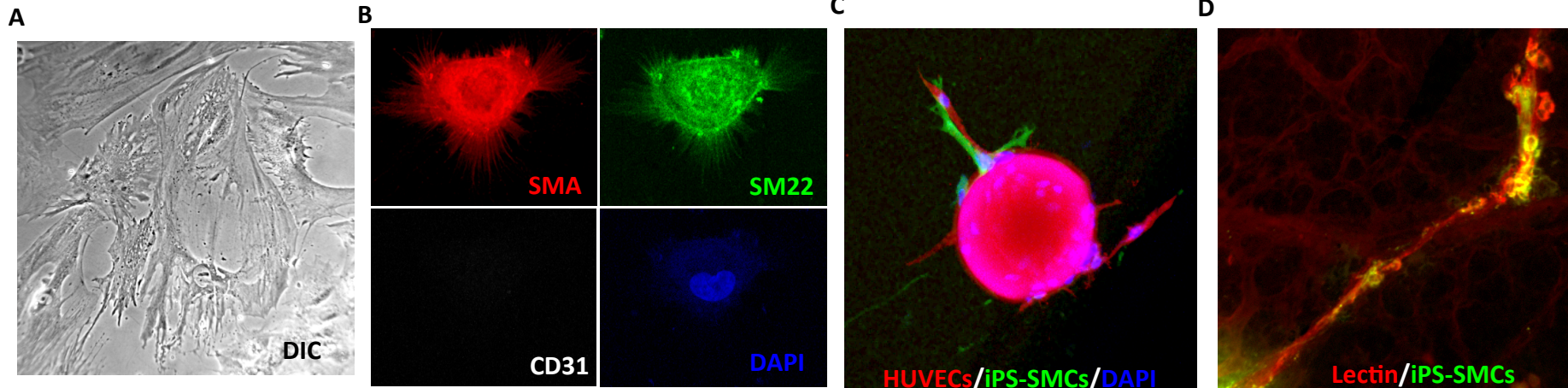


**Figure S4.** Characterization of hiPSC-derived SMCs. (A) Brightfield image of hiPSC-derived SMCs. (B) Immunocytochemistry analyses reveal that hiPSC-derived SMCs express smooth muscle cell markers SMA and SM22 but not the endothelial cell marker CD31. (C) Endothelial cells (red) grow from HUVEC coated beads in the presence of hiPSC-derived SMCs (green) in vitro. (D) Fluorescence labeled hiPSC-derived SMCs (green) can be associated with the GS Lectin positive hyaloidal vasculature network (red) two days after intravitreal injection in mouse pups (P14). (E) The expression of HLA-I,  $\beta$ 2M, HLA-DRB1, HLA-DQB1, and FASL in hiPSCs, human primary SMCs, hiPSC-derived SMCs and teratoma, was detected by qPCR. (F) The expression of TGF- $\beta$ 1 and IL-10 in human primary SMCs and hiPSC-derived SMCs was detected by qPCR. (G) The expression of Hormad1 in human primary SMCs and hiPSC-derived SMCs was detected by qPCR. Related to Figure 4.